Composites Science and Technology 159 (2018) 50–58

Contents lists available at ScienceDirect

Composites Science and Technology

journal homepage: http://www.elsevier.com/locate/compscitech

The dynamic mechanical properties of magnetorheological plastomers under high strain rate

Jiaqi Xu, Pengfei Wang, Haoming Pang, Yunpeng Wang, Jie Wu, Shouhu Xuan, Xinglong Gong*

CAS Key Laboratory of Mechanical Behavior and Design of Materials, Department of Modern Mechanics, University of Science and Technology of China, Hefei 230027, China

ARTICLE INFO

Article history:
Received 14 November 2017
Received in revised form
19 January 2018
Accepted 16 February 2018
Available online 21 February 2018

Keywords:
Magnetorheology
Split hopkinson pressure bar (SHPB)
Strain rate
Mechanical properties

ABSTRACT

The dynamic mechanical properties of magnetorheological plastomers (MRPs) were investigated by using a Split Hopkinson Pressure Bar (SHPB) equipped with an electromagnetic accessory. Both the SHPB and rheological test indicated the mechanical properties of MRPs increased with strain rate, which demonstrated the typical rate dependent stiffening performance. With strain rate increased from 1580 s^{-1} to 7900 s^{-1}, the maximum stress of MRPs increased from 31 MPa to 66 MPa. MRPs also exhibited a magnetic strengthening behavior due to the MR effect. Keeping the strain rate at 6500 s^{-1}, the maximum stress increased 19.8 MPa as the magnetic flux density increased from 0 to 480 mT and the increase rate of maximum stress reached to 34%. Moreover, a high-speed camera was also used to capture the deformation of MRPs in both low and high strain rates. Based on the above results, a possible mechanism was proposed to investigate the dynamic mechanical properties of the MRPs. The synergistic effect between the magnetic field dependent particle structure evolution and polymer chain deformation were responded for the MR behavior and strain rate stiffening characteristic, respectively.

1. Introduction

Magnetorheological (MR) materials are a class of intelligent composite materials prepared by dispersing micron or nanoscale magnetic particles within different matrixes. Because of the famous MR effect, their mechanical properties can be significantly influenced by external magnetic field. The MR materials have been attracted increasing research interests due to their high controllable and sensitive mechanical properties. During the past decades, many efforts have been conducted to apply them in the aspect of vibration control. These active dampers and vibration absorbers exhibited wide potential in vehicles [1,2], machineries [3,4], bridges [5,6], buildings [7,8], and other fields.

Depending on the matrix, the MR materials can be classified as magnetorheological fluids (MRFs), magnetorheological elastomers (MREs), and magnetorheological gels (MRGs). Recently, novel plastic MR materials named as magnetorheological plastomers (MRPs) were developed by doping ferromagnetic particles in the low cross-linking gel-like polyurethane (PU) [9]. Different from the MREs, the ferromagnetic particles inside MRPs were movable and they could change their position to form chains when an external magnetic field was applied. Because of their good stability, rapid response and high MR effect [10,11], the MRPs have received more and more attention. Till now, the mechanical properties of the MRPs under low strain rate, such as the compression performance [12], shear performance [13], creep and recovery [14], and shear dependent electrical performance have been intensively investigated [15,16]. Recently, a MRP based energy absorber was also developed and it was found that the MRP exhibited high performance in shock absorbing [17]. As we know, the dynamic properties of MRPs under high strain rate were fundamental for its application in shock absorbing. However, few work focused on the magnetic field dependent dynamic property of the MRPs was reported.

The split Hopkinson pressure bar (SHPB) played a key role in testing the dynamic mechanical properties of materials [18–20]. It can provide a dynamic load with a strain rate range of 10^2 s^{-1} to 10^4 s^{-1} [21,22]. The SHPB technology has been used to measure dynamic stress-strain curves in a variety of materials, such as metal foam [23,24], fiber [25,26], polymer [27,28], and composite

* Corresponding author.
E-mail address: gongxl@ustc.edu.cn (X. Gong).

https://doi.org/10.1016/j.compscitech.2018.02.030
0266-3538/

materials [29–31]. As a special particle strengthened composite, the dynamic mechanical property of MR materials should be also affected by the external magnetic field. Therefore, a modified SHPB equipped with electromagnet was developed and the dynamic compressive properties of both the MRF and MRE have been investigated [17,32]. It was also reported that the yield behavior of the magnetic shear thickening gel could be studied by the above SHPB [33]. Here, to further understand the detail working mechanism of MRPs based damper during the shock adsorbing, using SHPB to investigate the dynamic mechanical properties of the MRPs under high strain rate is necessary.

In this work, the dynamic mechanical properties of MRPs were tested by using a modified SHPB equipped with an electromagnetic accessory. The dynamic stress-strain curves of MRPs containing various weight fraction iron powders particles were measured under different strain rates. Moreover, the magnetic field response of MRPs at high strain rate compression testing was also investigated. The high-speed camera captured the deformation of MRPs in the high-strain-rate impact. Additionally, the microscopic evolution mechanism of MRPs under different magnetic flux density at various strain rates was also proposed.

2. Experiments

2.1. Materials and preparation

The raw materials of MRPs include polypropylene glycol (PPG-1000, Sinopec Group Co. Ltd, China), toluene diisocyanate (TDI, 2,4-TDI at B80%, 2,6-TDI at B20%, Tokyo Chemical Industry Co. Ltd, Japan), Diethylene glycol (DEG, Sinopharm Chemical Reagent Co. Ltd, Shanghai, China), carbonyl iron powders (CIPs, type CN, BASF aktiengesellschaft, Germany).

Firstly, TDI and PPG were added to the flask with a molar ratio of 3:1 at 80 °C for 2 h. Then, DEG was added into the reactor and the temperature was reduced to 60 °C. After 30 min, the homemade PU matrix was synthesized. The whole reaction was carried out under a continuous agitation. Before the matrix was cooled down, different amounts of CIPs were added into the matrix by vigorously stirring until they were mixed well. Then, the final MRPs with different CIP contents were obtained. For simplicity, the samples contained 20 wt%, 40 wt%, 60 wt%, 80 wt% CIPs that were named MRP-20, MRP-40, MRP-60, MRP-80 respectively.

2.2. Rheological tests of MRPs at different shear frequencies

The rheological tests of MRPs ($\Phi 20 \times 1$ mm) at different shear rates were performed by a commercial rheometer (Physica MCR301, Anton Paar Co., Austria) equipped with a magneto-controllable accessory MRD180. In this experiment, shear frequency increased from 1 Hz to 100 Hz and strain was kept at 0.1%. The MRD180 provided a variable magnetic flux density from 0 to 480 mT during test the magnetically responsive properties. The measurements were carried out at 25 °C.

2.3. Dynamic compression tests of the MRPs

A modified SHPB used for dynamic compression tests is illustrated in Fig. 1. The device consists of two parts. One part is traditional SHPB setup which mainly includes striker ($\Phi 14.5 \times 200$ mm), incident bar ($\Phi 14.5 \times 1000$ mm), transmission bar ($\Phi 14.5 \times 800$ mm), absorption bar ($\Phi 14.5 \times 600$ mm) and dashpot. The striker and the bars are made of aluminum. To reduce the dispersion of incident wave and modify the shape of the pulse, a pulse shaper was placed in the interface of the incident bar and the striker.

The other part is electromagnetic accessory which contains iron cores and magnetic coils. As the current increased from 0 A to 2 A, the magnetic flux density increased from 0 to 480 mT correspondingly. The sample was placed in the center of the magnetic device where the magnetic flux density was almost uniform.

According to the 1-D elastic wave propagation theory, the dynamic stress, the dynamic strain, and the strain rate can be expressed as:

$$\sigma_s = \frac{E_b A_b}{A_s}\varepsilon_t \tag{1}$$

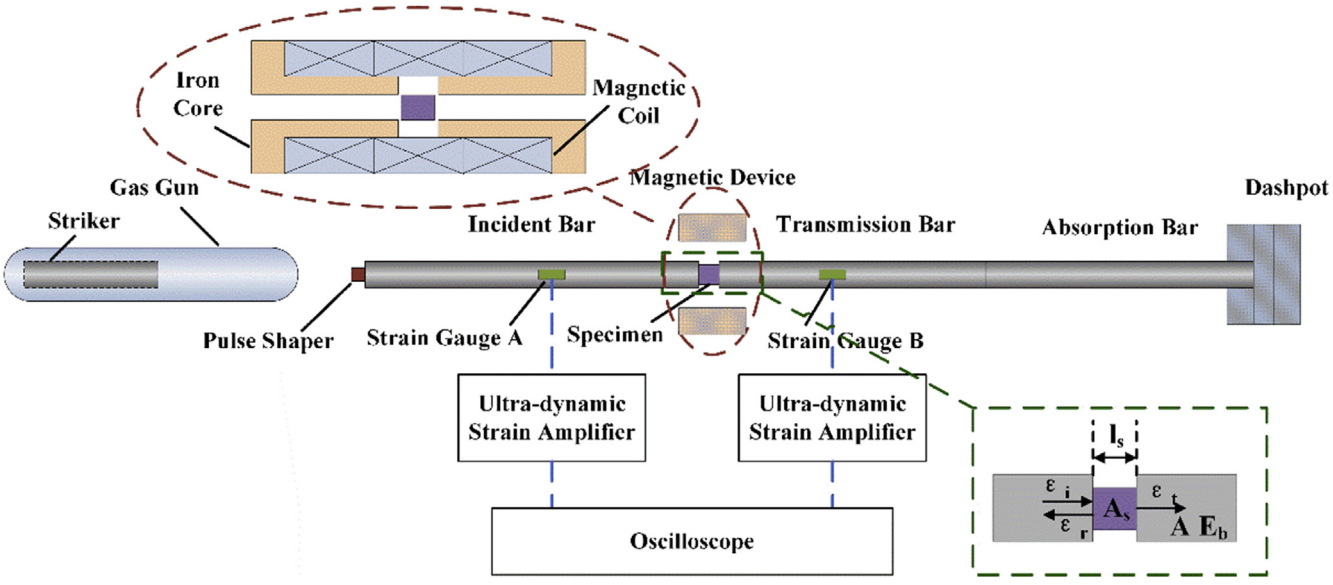

Fig. 1. Schematic of modified SHPB system for dynamic compression tests.

$$\varepsilon_s = \frac{2C_b}{l_s}\int_0^t (\varepsilon_i - \varepsilon_t)d\tau \quad (2)$$

$$\dot{\varepsilon_s} = \frac{2C_b}{l_s}(\varepsilon_i - \varepsilon_t) \quad (3)$$

where, σ_s, ε_s and $\dot{\varepsilon_s}$ are the dynamic stress, the dynamic strain and the strain rate respectively; ε_i and ε_t are the incident pulse and transmitted pulse, respectively. A_b and A_s are the cross-sectional areas of the samples and the bars respectively; E_b is the elastic modulus of the bar material. C_b is the propagation velocity of the elastic wave in the bar; l_s is the length of the sample.

3. Results and discussion

As shown in Fig. 2a, c, e and g were MRP-20, MRP-40, MRP-60 and MRP-80, the CIPs (20 wt%, 40 wt%, 60 wt% and 80 wt%, respectively) were uniformly dispersed within the matrix. When an external magnetic field was applied, the CIPs were assembled to form chain-like microstructures along the direction of the magnetic field (the blue arrow). This formation process of the CIPs chain-like structures in MRPs was named pre-configuration (Fig. 2b, d, f and

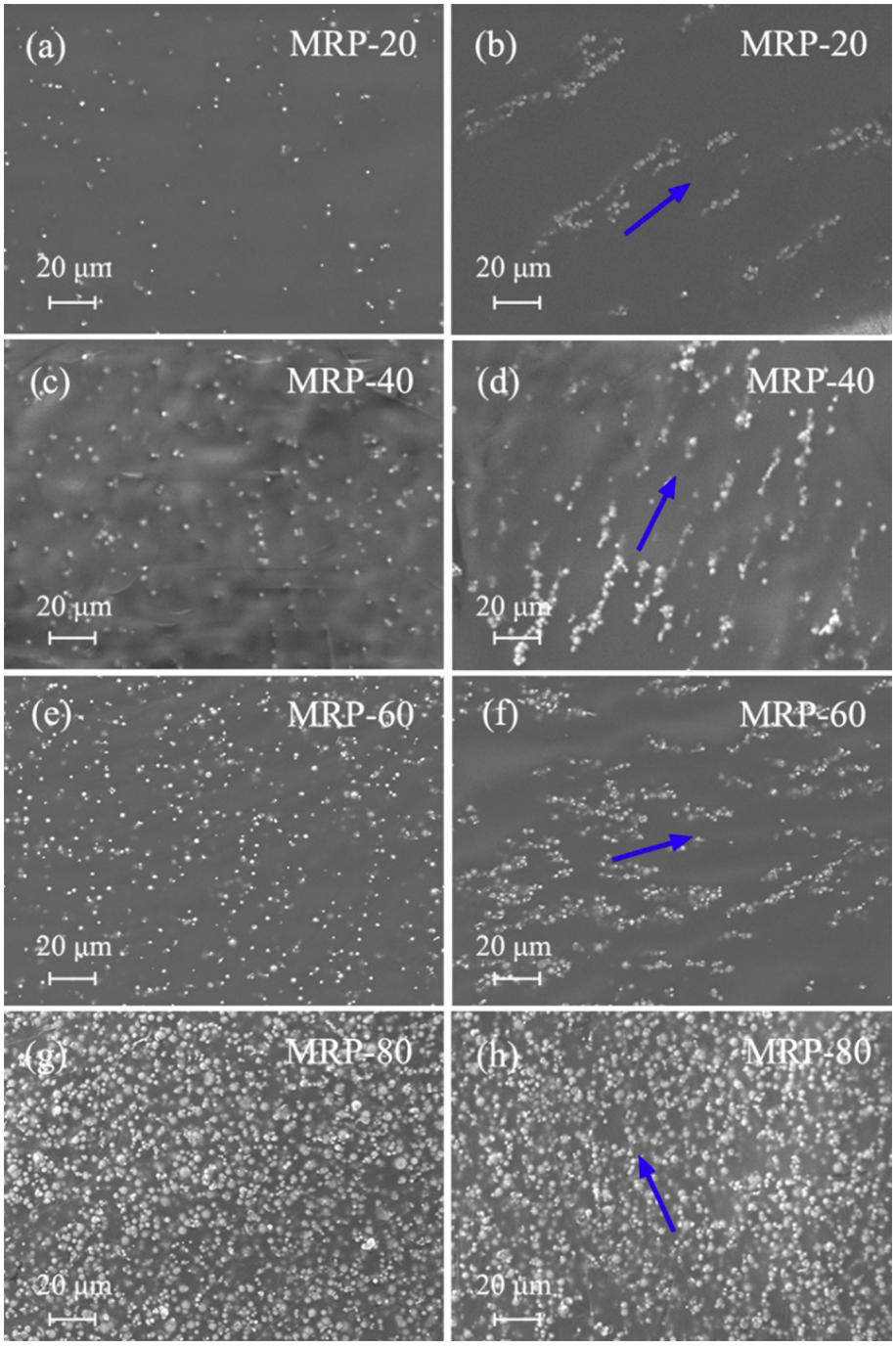

Fig. 2. The SEM images of MRPs (a), (c), (e), (g) without pre-configuration and (b), (d), (f), (h) after pre-configuration.

h). Clearly, the higher the weight fraction of the CIPs was, the denser the particles and the chains.

The mechanical properties of MRP were tested by a rheometer. Fig. 3 showed the storage modulus (G′) of the homemade PU with the shear frequency sweeping from 1 to 100 Hz. The G′ significantly increased from 9×10^2 Pa to 7×10^5 Pa, which improved three orders of magnitude. When frequencies were set at 1 Hz, 10 Hz, 100 Hz, G′ were maintained at 9×10^2 Pa, 5×10^4 Pa, 7×10^5 Pa, respectively. With increasing of the shear frequency, the storage modulus of the PU matrix increased, demonstrating a typical shear-stiffening performance. Here, the shear stiffening effect must be responded for the more tightly PU molecular chains wound with higher shear frequency.

The storage modulus of MRPs with different contents of CIPs under shear oscillation mode was measured. As shown in Fig. 4, similar to the PU matrix, with increasing of the frequency, the G′ of all MRPs increased, which exhibited the shear-stiffening performance. Here, the initial storage modulus of the MRPs increased with the CIP content, which must be originated from the particle strengthening effect. Although the final storage modulus also increased, their shear thickening effect decreased due to the higher increase of the initial storage modulus. For example, the G′ of MRP-20 increased from 2 kPa to 630 kPa with shear frequency rising from 1 Hz to 100 Hz, which increased about 30000%, but the G′ of MRP-80 increased from 0.3 MPa to 2.9 MPa, which increased only about 900% (Fig. 4a). As shown in Fig. 4b, the external magnetic field highly influenced the shear thickening behavior. Under applying the magnetic field, the particles in the MRPs assembled to form chain-like microstructure, which exhibited a higher strengthening effect than the uniformly dispersed CIPs. Therefore, the initial storage modulus of the MRPs was increased much faster than the final storage modulus. In this case, G′ of MRP-80 increased from 3.1 MPa to 3.2 MPa (increased about 3%) when the shear frequency was raised from 1 Hz to 100 Hz. Moreover, the low shear-stiffening property of the MRPs with high CIPs content under the magnetic field was because that the dense CIPs chains blocked the PU chains movement during the shear deformation.

To further investigate the MR property of the MRPs, the storage modulus of MRPs with different CIP contents under the different magnetic flux density was measured. As shown in Fig. 5, the storage modulus of MRPs increased with the magnetic flux density. For the low shear frequency (1 Hz), the G′ of MRP-60 increased from 0.05 MPa to 1.9 MPa with the magnetic flux density increased from 0 to 480 mT (Fig. 5a). The relative MR effects reached as high as 3800%. Besides the magnetic flux density, the storage modulus was also highly dependent on the content of CIPs. When the content of CIPs increased from 20 wt% to 80 wt%, the G′ of MRPs increased from 0.004 MPa to 0.29 MPa without magnetic field and 0.04 MPa–3.02 MPa with a 480 mT magnetic field. Fig. 5b showed the magnetic field dependent rheological property of the MRPs under high shear frequency (100 Hz). Clearly, the storage modulus of MRPs with different CIP contents were higher than the ones under low shear frequency. Nevertheless, the relative MR effects decreased due to the increase of initial storage modulus.

The dynamic compression properties of the MRPs under the different strain rates were measured using a modified SHPB system. Fig. 6a showed the stress-strain curves of MRP-60 at various strain rates. The compressive stress-strain curve was roughly divided into four parts: the elastic deformation region, the plastic beginning deformation region, the plastic instability deformation region, the unloading region. In elastic deformation region, the stress almost linearly increased with the strain. Secondly, the stress grew non-linearly with the strain and the slope suddenly decreased, and it was named as the plastic beginning deformation region. When the increase trend of the stress slowed down, the sample reached the plastic instability deformation region and then the sample was unloaded. In the interior of the sample, the CIPs introduced the local stress concentration, so the sample exhibited plastic instability in the plastic deformation region [34]. It was also found that the compressive stress of the MRPs was highly dependent on the

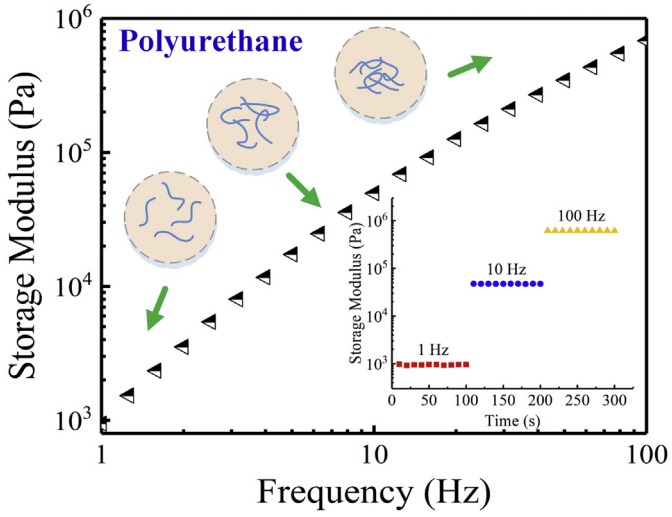

Fig. 3. The storage modulus of the matrix (PU) with the shear frequency sweeping.

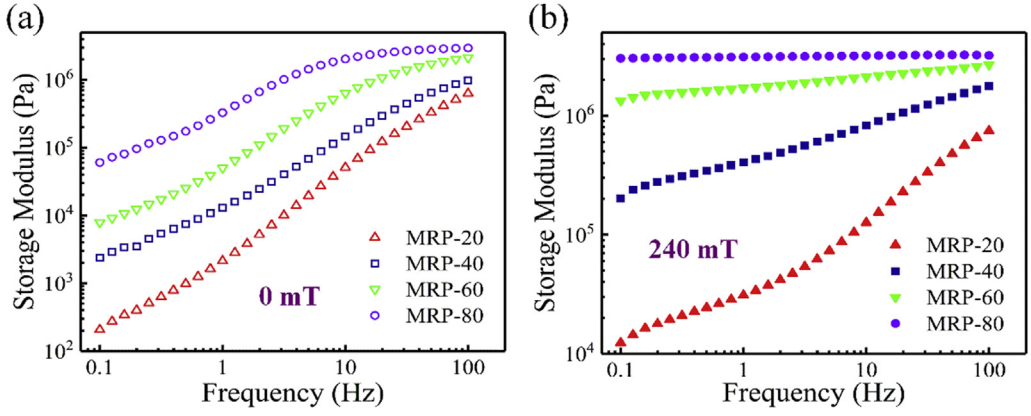

Fig. 4. The shear frequency sweeping tests of MRPs with different contents of CIPs: (a) without magnetic field; (b) with 240 mT magnetic field.

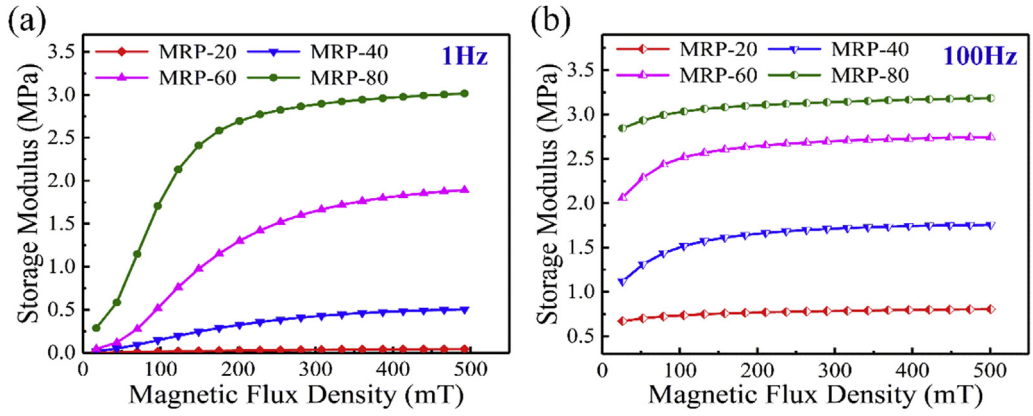

Fig. 5. The storage modulus of MRPs under the different magnetic flux density. The shear frequency was (a) 1 Hz and (b) 100 Hz, respectively.

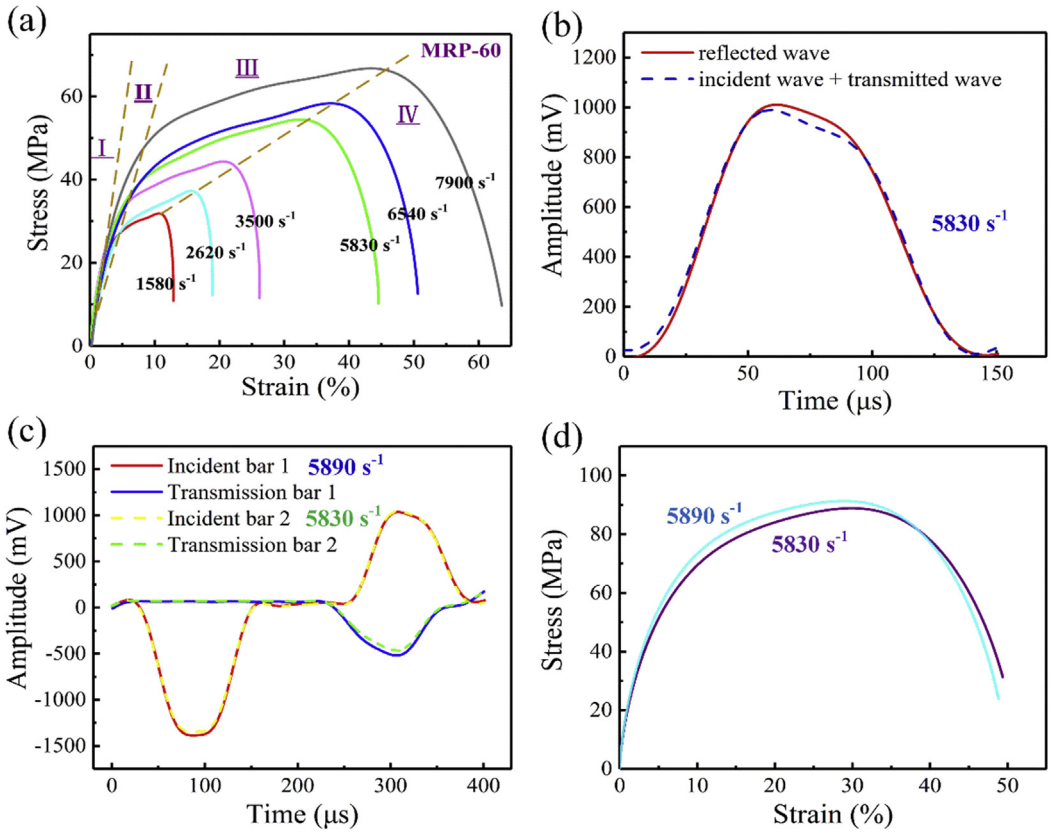

Fig. 6. (a) Dynamic compressive stress-strain curves of MRP-60 at different strain rates; (b) stress equalization analysis; (c) the typical pulse-shaped and (d) the stress-strain curves of primary sample and reshaped sample.

strain rate. As shown in Fig. 6a, the stress increased from about 31 MPa to 66 MPa with the strain rate increased from 1580 s^{-1} to 7900 s^{-1}, which clearly represented the rate sensitivity and the stiffening property.

Stress equalization was important for polymer materials in dynamic compression test [27]. According to the wave propagation theory, the incident pulse ε_i, reflected pulse ε_r and transmitted pulse ε_t followed a relationship as shown: $\varepsilon_i + \varepsilon_r = \varepsilon_t$. As Fig. 6b shown, the theoretical ε_r was consistent with the reflected wave signal collected by the strain gauge. The sample reached the stress equalization in dynamic compression tests with SHPB system. The repeatability of MRPs under high strain rate test were also studied. After the first test, the sample was removed and kneaded back into the test area for the second test with the strain rate of about 5800 s^{-1}. Fig. 6c and d respectively showed the pulse-shape and the corresponding stress-strain curves. The waveforms and stress-strain curves obtained by repeated experiments were very similar.

In order to further analyze the deformation of MRPs under dynamic compression, a high-speed camera was used to capture the deformation of MRPs. MRP-60 with a thickness of 2 mm was placed between the incident bar and the transmission bar (Fig. S1). As shown in Fig. 7, the sample underwent a slight deformation at a lower strain rate. When the strain rate reached 7900 s^{-1}, a large radial deformation was observed in the test sample. No obvious

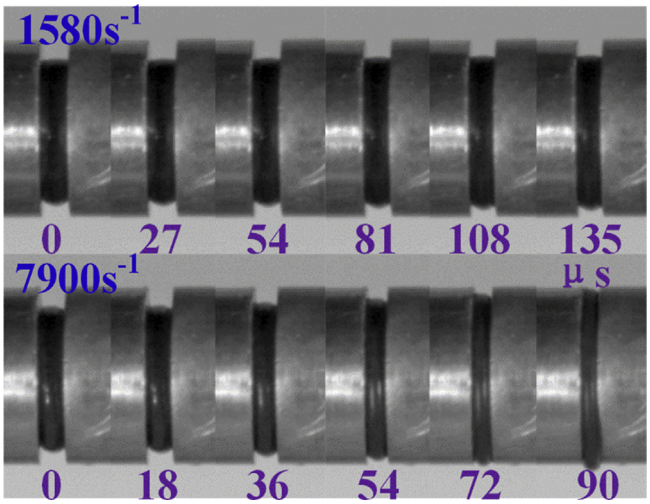

Fig. 7. The dynamic compression process of MRP-60 recorded by high-speed camera.

cracks were observed in high-speed photography due to the high viscosity of the matrix and good interfacial properties [35]. However, there may also be many minor crazings in the interior of the matrix that have not developed into cracks [36]. These minor crazings formed a plastic zone which contributed to the impact toughness [27].

Fig. 8a showed the effect of strain rate on the dynamic compression stress-strain curves of MRPs with different CIP contents. Here, the CIP contents were varied from 20 wt% to 40 wt%, 60 wt%, and 80 wt%, and the strain rates were set at about 1500 s^{-1}, 3500 s^{-1}, and 6500 s^{-1}. With increasing of the CIP contents and strain rates, the stress increased. As shown in Fig. 8b, when the content of the CIP increased from 20 wt% to 80 wt%, the stress of MRPs with a 10% strain rose from 13 MPa to 56 MPa at the strain rate of about 1500 s^{-1}, from 23 MPa to 69 MPa at the strain rate of about 3500 s^{-1}, and from 26 MPa to 75 MPa at the strain rate of about 6500 s^{-1}. The particle enhancement effect was higher under a larger CIP content, which further strengthened the MRPs. Otherwise, at higher strain rate, the PU molecular chains were tightly wound together with the CIPs, which produced a synergistic effect on the enhancement of the stress. Fig. 8c and d showed the evolution of the strain rate over the time. The strain rates rose rapidly at about 30 μm due to the impact of the bullet. Then the strain rates were almost stable until the sample was unloaded. The deformation of samples was uniform at low and medium strain rates, whereas accelerated at high strain rates.

The dynamic compression tests of MRPs with different CIP contents under a 240 mT magnetic field were measured. The strain rates were about 2200 s^{-1} and 5500 s^{-1}. Fig. 9a clearly showed that the stress increased with the CIP content. Under the strain rate of about 2200 s^{-1}, the stress increased from 13 MPa to 68 MPa at the one strain (10%) with the CIP content increased from 20 wt% to 80 wt%. When the strain rate reached about 5500 s^{-1}, the stress increased from 20 MPa to 73 MPa (Fig. 9b). Under applying an external magnetic field, more CIPs were assembled to form denser chain-like structures, which further enhanced the mechanical properties.

The influence of magnetic field on dynamic compression stress was carried out. Fig. 10a and b showed the stress-strain curves of MRP-60 at the strain rate of about 2200 s^{-1} and 6500 s^{-1}. The

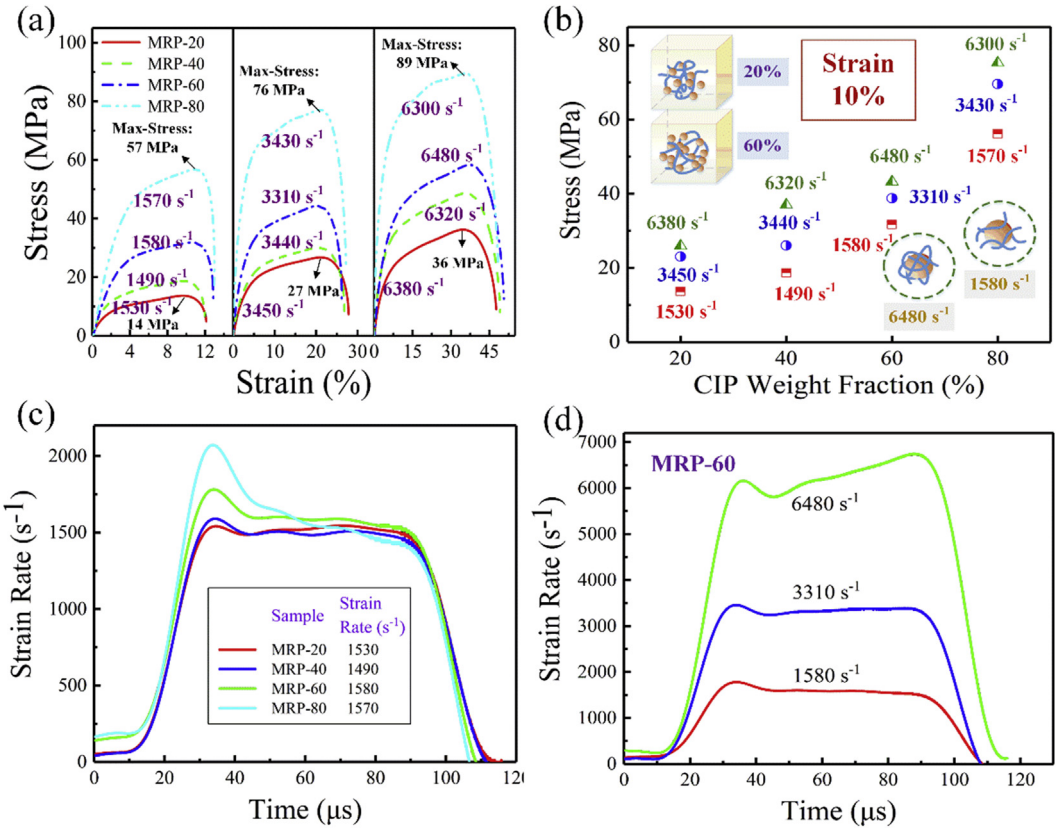

Fig. 8. (a) The stress-strain curves of MRPs at the different strain rates; (b) the stress of MRPs at 10% strain; (c) and (d) the strain rate vs times of MRPs with different CIP contents and strain rates.

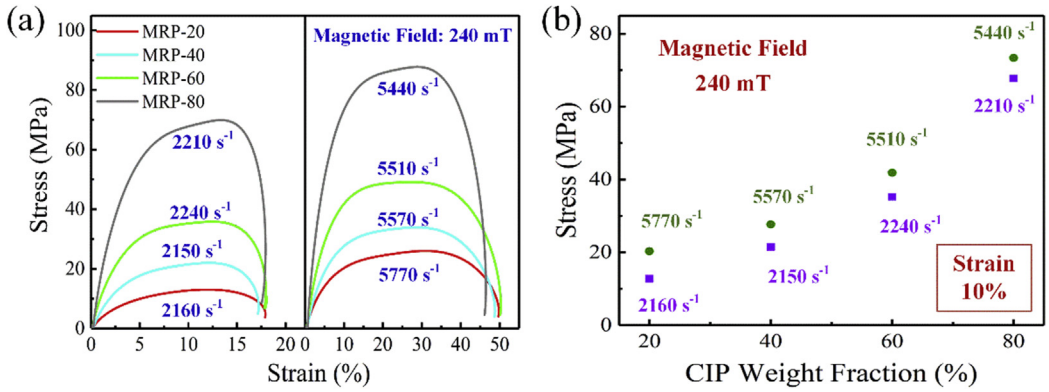

Fig. 9. (a) The dynamic compression stress-strain curves of MRPs under the magnetic field; (b) the stress of MRPs at 10% strain.

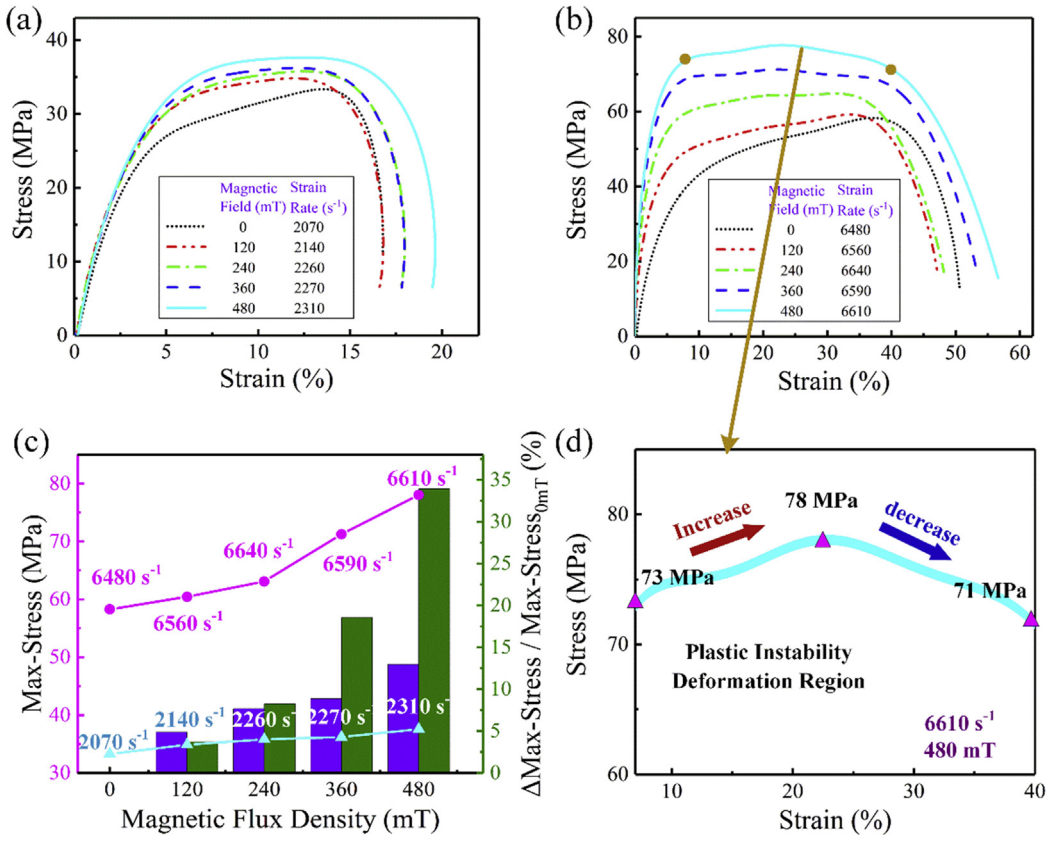

Fig. 10. The dynamic compression stress-strain curves of MRP-60 with different magnetic field at the strain rate of about (a) 2200 s^{-1} and (b) 6500 s^{-1}. (c) The maximum stress and the increase rate of maximum stress of MRP-60 (d) The plastic instability deformation region of dynamic compression stress-strain curves of MRP-60.

dynamic compression stress increased with strain rate and magnetic flux density. Fig. 10c showed the maximum stress and the increase rate of maximum stress of MRP-60. Due to the limited length of the bullet in the SHPB device, the duration of the loading pulse was fixed and limited, which resulted in the sample being unable to load into the fracture at the current loading rate [27].

By increasing the magnetic flux density from 0 to 480 mT, the maximum stress increased 4.3 MPa and 19.8 MPa at the strain rate of about 2200 s^{-1} and 6500 s^{-1}. The increase rate of maximum stress under a lower magnetic field (120 mT) was 5% at 2140 s^{-1} and 4% at 6560 s^{-1}, indicated a decreasing nature. Inversely, under a higher magnetic field, the increase rate of maximum stress at about 6500 s^{-1} was larger than the one at about 2200 s^{-1}. As soon as the magnetic flux density reached 480 mT, the increase rate of maximum stress was 34% at the strain rate of 6610 s^{-1}, and only 13% at the strain rate of 2310 s^{-1}. With the magnetic field increasing, the chain-like structures were stronger, which strengthened MRPs. Moreover, the matrix was also stiffened due to the entanglement of the polymer molecular chains at the high strain rate, which also contributed to the increase of stress (Fig. 3). In case of lower strain rate, the polymer molecular chains were stretched and the matrix was soft so that the CIPs could move freely. Conversely, at high strain rates, the molecular chains of the matrix were tightly entangled with the CIPs thus the particles were subjected to great resistance to the movement. Given that, CIPs were easy to form chain-like structures at a lower strain rate, and macroscopically the

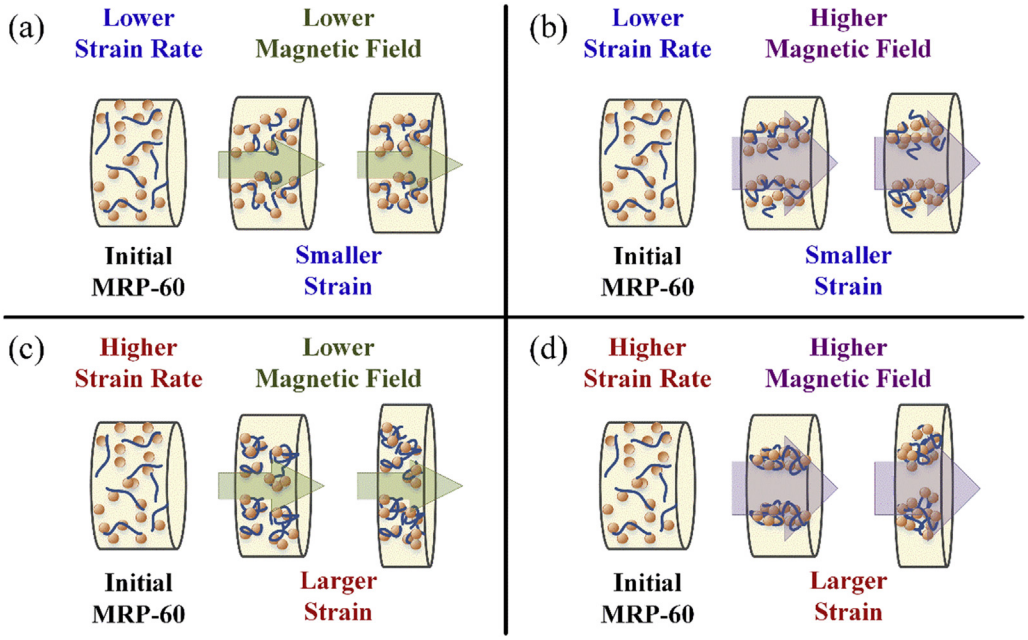

Fig. 11. The microstructure evolution of MRPs in dynamic compression process.

greater the increase rate of stress was. As for a higher strain rate, the increase rate of stress was greater only if the magnetic field force was larger enough to make the CIPs overcome the entanglement of the matrix molecular chain.

Fig. 10d showed the plastic instability deformation region of dynamic compression stress-strain curve of the MRP-60 with a 480 mT magnetic field at the strain rate of 6610 s^{-1}. The stress increased from 73 MPa to 78 MPa firstly, and then decreased to 71 MPa. In plastic instability deformation region, the stress decreased 2 MPa. It was found that only when the MRPs were stayed in higher magnetic field and higher strain rate, the stress could decrease in the plastic instability deformation region (Fig. S3).

Fig. 11 proposed a possible microstructure evolution of MRPs in dynamic compression test. The orange balls represented the CIPs. The blue lines represented the PU molecular chains [9,37]. At lower strain rate, the stiffening performance of matrix was not significant (Fig. 3), and the CIPs were easily assembled to form chains in a magnetic field (Fig. 11a). With increasing of magnetic flux density, the spacing between CIPs reduced and the chain-like microstructures became more obvious (Fig. 11b) [37]. In other words, the magnetic field can improve the mechanical properties of MRPs (Fig. 10a).

At a higher strain rate, the CIPs were tightly entangled by the PU molecular chains (Fig. 3) [38], and they were difficult to aggregate to chain-like microstructures under the low magnetic flux density (Fig. 11c). Therefore, the increase rate of maximum stress with higher strain rate was smaller than the one with lower strain rate under a low magnetic field (such as 120 mT, Fig. 10c). When magnetic flux density increased, the CIPs overcame the matrix constraints and then aggregated to form chains along the direction of magnetic field (Fig. 11d). That was why the increase rate of maximum stress was improved under the higher magnetic flux density (such as 240 mT–480 mT, Fig. 10c).

Otherwise, the sample underwent a minor strain at a lower strain rate. The slight compression deformation promoted the CIPs more closely (Fig. 11a). However, at higher strain rates, the deformation of MRPs was serious. The chain-like microstructures formed under high magnetic flux density were damaged due to the large strain (Fig. 11d). It exhibited a negative effect on mechanical properties, so the stress of MRPs decreased in plastic instability deformation region at large magnetic field and high strain rate (Fig. 10d).

4. Conclusions

In this study, the dynamic compression properties of MRPs were studied by a modified SHPB. The stress of MRPs increased 35 MPa with the strain rate increases from 1580 s^{-1} to 7900 s^{-1}, which indicated that MRPs had a stiffening property on the impact. When an external magnetic field was applied, the stress of MRPs increased with the magnetic flux density. The increase rate of maximum stress reached to 34%, demonstrated an excellent MR effect. The possible microstructure evolution of MRPs under different strain rates and magnetic flux density was discussed. Under a high magnetic flux density, the CIPs within MRPs were easily to overcome the constraints of polymer molecular chain and form tight chains, which enhanced mechanical property. However, the particle chains could be broken under a big deformation. Therefore, the storage modulus of MRPs slightly decreased with the high strain rate and high magnetic flux density.

Acknowledgements

Financial supports from the National Natural Science Foundation of China (Grant No. 11572309, 11572310), the Strategic Priority Research Program of the Chinese Academy of Sciences (Grant No. XDB22040502), and the Fundamental Research Funds for the Central Universities (WK2480000002) are gratefully acknowledged. This study was also supported by the Collaborative Innovation Center of Suzhou Nano Science and Technology.

Appendix A. Supplementary data

Supplementary data related to this article can be found at https://doi.org/10.1016/j.compscitech.2018.02.030.

References

[1] H. Du, J. Lam, K. Cheung, W. Li, N. Zhang, Direct voltage control of magneto-rheological damper for vehicle suspensions, Smart Mater. Struct 22 (10) (2013), 105016.

[2] D.K. Shin, S.-B. Choi, Design of a new adaptive fuzzy controller and its application to vibration control of a vehicle seat installed with an MR damper, Smart Mater. Struct. 24 (8) (2015), 085012.

[3] G. Hu, M. Liao, W. Li, Analysis of a compact annular-radial-orifice flow magnetorheological valve and evaluation of its performance, J. Intell. Mater. Syst. Struct. 28 (10) (2017) 1322–1333.

[4] M. Brigley, Y.-T. Choi, N.M. Wereley, S.-B. Choi, Magnetorheological isolators using multiple fluid modes, J. Intell. Mater. Syst. Struct. 18 (12) (2007) 1143–1148.

[5] A. YeganehFallah, N.K.A. Attari, Robust control of seismically excited cable stayed bridges with MR dampers, Smart Mater. Struct. 26 (3) (2017), 035056.

[6] M.-G. Yang, C.S. Cai, Longitudinal vibration control for a suspension bridge subjected to vehicle braking forces and earthquake excitations based on magnetorheological dampers, J. Vib. Contr. 22 (17) (2016) 3659–3678.

[7] Y.-J. Cha, A.K. Agrawal, Seismic retrofit of MRF buildings using decentralized semi-active control for multi-target performances, Earthq. Eng. Struct. Dynam. 46 (3) (2017) 409–424.

[8] J.W. Chong, Y. Kim, K.H. Chon, Nonlinear multiclass support vector machine–based health monitoring system for buildings employing magnetorheological dampers, J. Intell. Mater. Syst. Struct. 25 (12) (2014) 1456–1468.

[9] Y. Xu, X. Gong, S. Xuan, W. Zhang, Y. Fan, A high-performance magnetorheological material: preparation, characterization and magnetic-mechanic coupling properties, Soft Matter 7 (11) (2011) 5246–5254.

[10] S. Xuan, Y. Xu, T. Liu, X. Gong, Recent progress on the magnetorheological plastomers, Int. J. Smart Nano Mater 6 (2) (2015) 135–148.

[11] Y. Xu, X. Gong, S. Xuan, Soft magnetorheological polymer gels with controllable rheological properties, Smart Mater. Struct. 22 (7) (2013), 075029.

[12] T. Liu, Y. Xu, X. Gong, H. Pang, S. Xuan, Magneto-induced normal stress of magnetorheological plastomer, AIP Adv. 3 (8) (2013), 082122.

[13] T. Liu, X. Gong, Y. Xu, H. Pang, S. Xuan, Magneto-induced large deformation and high-damping performance of a magnetorheological plastomer, Smart Mater. Struct. 23 (10) (2014), 105028.

[14] Y. Xu, X. Gong, S. Xuan, X. Li, L. Qin, W. Jiang, Creep and recovery behaviors of magnetorheological plastomer and its magnetic-dependent properties, Soft Matter 8 (32) (2012) 8483.

[15] J. Xu, S. Xuan, H. Pang, X. Gong, The strengthening effect of 1D carbon materials on magnetorheological plastomers: mechanical properties and conductivity, Smart Mater. Struct. 26 (3) (2017), 035044.

[16] H. Pang, S. Xuan, T. Liu, X. Gong, Magnetic field dependent electroconductivity of the graphite doped magnetorheological plastomers, Soft Matter 11 (34) (2015) 6893–6902.

[17] G. Liao, X. Gong, S. Xuan, Magnetic field-induced compressive property of magnetorheological elastomer under high strain rate, Ind. Eng. Chem. Res. 52 (25) (2013) 8445–8453.

[18] H. Gu, Y. Guo, S.Y. Wong, C. He, X. Li, V.P.W. Shim, Effect of interphase and strain-rate on the tensile properties of polyamide 6 reinforced with functionalized silica nanoparticles, Compos. Sci. Technol. 75 (2013) 62–69.

[19] M. Tarfaoui, S. Choukri, A. Neme, Effect of fibre orientation on mechanical properties of the laminated polymer composites subjected to out-of-plane high strain rate compressive loadings, Compos. Sci. Technol. 68 (2) (2008) 477–485.

[20] S. ZhenHua, W. ZhiHua, M. HongWei, X. HaiJun, Mechanical behavior and failure mode of woven carbon/epoxy laminate composites under dynamic compressive loading, Compos. B Eng. 60 (2014) 531–536.

[21] A. Gilat, R.K. Goldberg, G.D. Roberts, Experimental study of strain-rate-dependent behavior of carbon/epoxy composite, Compos. Sci. Technol. 62 (10–11) (2002) 1469–1476.

[22] Z. Jia, D. Hui, G. Yuan, J. Lair, K.-t. Lau, F. Xu, Mechanical properties of an epoxy-based adhesive under high strain rate loadings at low temperature environment, Compos. B Eng. 105 (2016) 132–137.

[23] P. Li, N.V. Nguyen, H. Hao, Dynamic compressive behaviour of Mg foams manufactured by the direct foaming process, Mater. Des. 89 (2016) 636–641.

[24] B. Zhang, Y. Lin, S. Li, D. Zhai, G. Wu, Quasi-static and high strain rates compressive behavior of aluminum matrix syntactic foams, Compos. B Eng. 98 (2016) 288–296.

[25] H. Cui, D. Thomson, A. Pellegrino, J. Wiegand, N. Petrinic, Effect of strain rate and fibre rotation on the in-plane shear response of +/- 45 degrees laminates in tension and compression tests, Compos. Sci. Technol. 135 (2016) 106–115.

[26] R. Kapoor, L. Pangeni, A.K. Bandaru, S. Ahmad, N. Bhatnagar, High strain rate compression response of woven Kevlar reinforced polypropylene composites, Compos. B Eng. 89 (2016) 374–382.

[27] J.T. Fan, J. Weerheijm, L.J. Sluys, Dynamic compressive mechanical response of a soft polymer material, Mater. Des. 79 (2015) 73–85.

[28] J.T. Fan, J. Weerheijm, L.J. Sluys, Glass interface effect on high-strain-rate tensile response of a soft polyurethane elastomeric polymer material, Compos. Sci. Technol. 118 (2015) 55–62.

[29] D.-s. Li, H.-r. Chen, D.-y. Ge, N. Jiang, L. Jiang, Split Hopkinson pressure bar testing of 3D multi-axial warp knitted carbon/epoxy composites, Compos. B Eng. 79 (2015) 692–705.

[30] M. Zhang, J. Chen, C. Lu, Influence of strain rate on the piezoresistive behavior of conductive polyamide composites, Compos. Sci. Technol. 133 (2016) 1–6.

[31] D. Li, H. Duan, W. Wang, D. Ge, L. Jiang, Q. Yao, Strain rate and temperature effect on mechanical properties and failure of 3D needle-punched Carbon/Carbon composites under dynamic loading, Compos. Struct. 172 (2017) 229–241.

[32] L. Fras, The perzyna viscoplastic model in dynamic behaviour of magneto-rheological fluid under high strain rates, Eng. Trans. 63 (2) (2015) 233–243.

[33] Y. Wang, S. Wang, C. Xu, S. Xuan, W. Jiang, X. Gong, Dynamic behavior of magnetically responsive shear-stiffening gel under high strain rate, Compos. Sci. Technol. 127 (2016) 169–176.

[34] A. Jumahat, C. Soutis, F.R. Jones, A. Hodzic, Effect of silica nanoparticles on compressive properties of an epoxy polymer, J. Mater. Sci. 45 (21) (2010) 5973–5983.

[35] J.T. Fan, J. Weerheijm, L.J. Sluys, Compressive response of multiple-particles-polymer systems at various strain rates, Polymer 91 (2016) 62–73.

[36] J.T. Fan, J. Weerheijm, L.J. Sluys, High-strain-rate tensile mechanical response of a polyurethane elastomeric material, Polymer 65 (2015) 72–80.

[37] P. Yang, M. Yu, J. Fu, S. Liu, S. Qi, M. Zhu, The damping behavior of magnetorheological gel based on polyurethane matrix, Polym. Compos. 38 (7) (2017) 1248–1258.

[38] Y. Tian, H. Zhang, J. Zhao, T. Li, B.-X. Bie, S.-N. Luo, Z. Zhang, High strain rate compression of epoxy based nanocomposites, Composer Part A Appl. S 90 (2016) 62–70.